Noise Reduction of a Rocket Payload Fairing Using Tuned Vibration Absorbers with Translational and Rotational DOFs

Carl Q. Howard , Colin H. Hansen, and Anthony C. Zander

School of Mechanical Engineering, The University of Adelaide, Adelaide, SA 5005, Australia

ABSTRACT

Numerical optimisations were conducted to reduce the noise levels inside the payload bay of a rocket by using vibration and acoustic absorbers attached to the fairing walls. The vibration absorbers act in both translational and rotational axes. The acoustic absorbers were modelled as simplified Helmholtz resonators. A Finite Element model of the vibro-acoustic system was created in ANSYS and the uncoupled structural and acoustic modal responses were calculated. The combined response of the acoustic and vibration absorbers, the acoustic cavity and structural modal responses were coupled using modal coupling theory in Matlab. The optimisation of the parameters and locations of the absorbers were conducted using a semi-synchronous parallel genetic algorithm and a large number of networked desktop computers.

INTRODUCTION

The work described here is part of a multi-stage project with the US Airforce to investigate passive means of improving the noise reduction of rocket vehicle fairings that are used to launch satellites into space. The noise levels during launch can reach 140dB re 20µPa on the exterior of a payload bay. Developments in materials technology have enabled the use of composite materials for fairings that reduces the weight of fairing, but also decreases the noise reduction qualities of the fairing compared to the use of heavier aluminium fairings. The cost to launch payloads into space is estimated to be between $US20,000 and $US40,000 per kilogram (Futron, 2002). Excessive noise levels inside the payload bays of launch vehicles are blamed for as many as 60% of first day satellite failures (Griffin et al., 2000). It is estimated that 40% of the weight of a satellite is required just to survive the launch environment (Henderson et al., 2003). Hence, there are significant benefits in reducing the weight of the rocket and satellite, both in terms of reducing the cost to launch satellites, and also reducing the risk of damage to the satellite caused by excessive noise and vibration during launch.

Howard et al. (2005) describe a computational tool for predicting the noise levels inside the cavity of a vibro-acoustic system, which includes optimising the parameters of passive acoustic absorbers and passive vibration dampers attached to the walls of the structure. The tool makes use of a semi-synchronous parallel genetic algorithm (Goldberg, 1999), which operates on a distributed computing network, to calculate the optimum locations and parameters of the absorbers that result in the minimisaton of the acoustic potential energy within the acoustic cavity. The acoustic potential energy within the cavity is calculated by using modal-coupling theory that was implemented using Matlab software. Finite element analysis is used to calculate the uncoupled vibration modes of the structure and the acoustic modes of the cavity, and these modal data are used with the Matlab modal coupling software to calculate the coupled vibro-acoustic response of the system. The advantage of using finite element analysis is that it enables complex shaped objects to be analysed, such as the composite payload fairing examined here.

The Representative Scaled Launch Vehicle Fairing (RSLVF), shown in Figure 1, is an example of a payload fairing that is made from light-weight composite materials. The fairing is about 2m in diameter and 5m long. Passive tuned dampers (TMDs) and passive Helmholtz resonators (HRs) can be combined into a single device to form a Passive Vibro-Acoustic Device (PVAD). These PVADs can be placed on the walls of the fairing to improve its noise reduction.
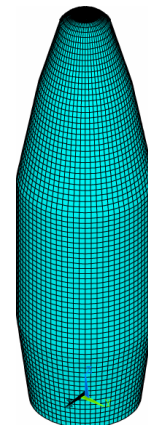

Figure 1: Finite element model of the RSLVF.

The work presented here begins with a description of a mathematical model for the coupling of a multi-degree-of-freedom TMD that includes both translational and rotational degrees of freedom to an underlying structure. The optimisation of the parameters for the PVADs requires the use of extensive computational resources. It demonstrated that extensive computational resources can be created by networking desktop computers to solve complex optimisation problems relatively easily.

MODELLING

The equations for the coupled vibro-acoustic response of a system are described by Fahy (1994) and have been implemented in Matlab software described in Howard et al. (2005).

Equations of Motion for Moment Loading on Shells

Most vibrational analyses ignore the contribution due to rotational degrees of freedom as it is frequently considered to be less important than the contribution from translational degrees of freedom. However, recent work has shown that the contribution of rotational degrees of freedom on shell structures often plays a significant part in vibrational power transmission and cannot be ignored (Howard, 1999).

As multiple degree of freedom vibration dampers transmit both forces and moments on the structure, the equations of motion of the structure must include these loads. This section contains the derivation of the equations of motion of thin shelled structures excited by both translational forces and rotational moments. The theory is developed using Soedel (1993) and Howard (1999).

The theoretical development of the application of multiple degree of freedom PVADs to the structure is very similar to existing theoretical models of vibration isolated platforms attached to flexible structures. It is useful to start the development of this framework with a numerical model of the flexible structure, similar to the existing theoretical models, and then in the final stages of the development, the modal results from the finite element analysis can be substituted for the theoretical modal results.

Multiple PVADs are attached to the fairing and each PVAD applies a force to it that can be described in a cylindrical coordinate system as

$$\mathbf{Q}_J = \begin{bmatrix} F_{xJ} & F_{\theta J} & F_{rJ} & M_{xJ} & M_{\theta J} & M_{rJ} \end{bmatrix}^{\mathrm{T}} \quad (1)$$

where $J = 1 \ldots L_1$, and there are L_1 PVADs attached to the fairing. Forces are transmitted into the structure along the axis of the fairing F_{xJ}, tangential to the surface $F_{\theta J}$, and radially F_{rJ}. Moments are transmitted into the structure and are described using the right-hand-rule about the axis of the fairing M_{xJ}, tangential to the surface of the fairing $M_{\theta J}$, and a drilling moment normal to the fairing M_{rJ}.

The force and moment components in $\mathbf{Q}_J$ are assumed to be concentrated point actions at the joint between the fairing at PVAD location σ_J on the thin shell, so that Dirac Delta functions δ and their partial derivatives can be used to describe the external force distribution on the fairing.

The motion of the fairing can be described by the Donnell-Mushtari thin-shell theory (Leissa, 1973) which uses eighth order differential equations. These equations can be simplified if the radius R of the shell is significantly large compared to the shell thickness h. In this case the vibration of the fairing is primarily radial, with the axial x and tangential θ displacements being small enough to allow the corresponding inertia terms in the axial and tangential directions in the equation of motion of the fairing to be neglected. Forces acting in the axial x and tangential θ directions excite vibration in these directions which in turn couple with the radial vibration to produce vibration in the radial w direction but at a much smaller amplitude. The radial vibration amplitude produced in this way is considered small compared to the radial vibration produced directly by moments and radial forces.

Note that the axial and tangential forces produced on the inside surface of the fairing produce moments about the mid-surface of the shell which result in direct excitation of radial motion. This is taken into account in the following analysis.

The response of the fairing can be described as (Soedel, 1993)

$$\ddot{\eta}_k + 2\xi_k \omega_k \dot{\eta}_k + \omega_k^2 \eta_k = F_k \quad (2)$$

where η_k is the kth modal participation factor, ξ_k is the viscous damping coefficient of the shell at the kth mode, ω_k is the resonance frequency of the kth mode, and F_k is the kth modal force which is applied to the shell for and is defined as

$$F_k = \frac{1}{\rho h N_k} \int_0^{2\pi} \int_0^{\frac{L}{R}} \left\{ \begin{array}{l} q_s U_{sk} + q_\theta U_{\theta k} + q_w U_{wk} \\ + \dfrac{U_{sk}}{2R} \dfrac{\partial(-T_n)}{\partial \theta} \\ - \dfrac{U_{\theta k}}{2R} \dfrac{\partial(-T_n)}{\partial s} \\ + \dfrac{U_{\theta k}}{2R} T_s + \dfrac{U_{wk}}{R^2} \\ \left[\dfrac{\partial(-T_\theta R)}{\partial s} + \dfrac{\partial(T_s R)}{\partial \theta} \right] \end{array} \right\} R^2 \, ds \, d\theta \quad (3)$$

where L is the length of the shell, q_i and T_i represent the forces and moments applied along each of the three axes, defined as

$$q_{iJ} = \frac{F_{iJ}}{R^2} \delta(s - s_J) \delta(\theta - \theta_J) e^{j\omega t} \quad (4)$$

$$T_{iJ} = \frac{M_{iJ}}{R^2} \delta(s - s_J) \delta(\theta - \theta_J) e^{j\omega t} \quad (5)$$

where F_i and M_i are the forces and moments applied to the shell at location σ_J in the directions $i = s$, θ, w, U_{ik} is the modal response in the ith direction, δ is the Dirac delta function and

$$N_k = \int_0^{2\pi} \int_0^{\frac{L}{R}} \left\{ U_{1k}^2 + U_{2k}^2 + U_{3k}^2 \right\} R^2 \, ds \, d\theta \quad (6)$$

Equation (3) is not the same as printed in Soedel (1996). It was found by Howard (1999) that terms were missing which account for the moment loading on the shell. This has been corrected in Eq. (3) shown here. A detailed description of the correction is given in Howard (1999).

The terms on the left hand side of the integral in Eq. (3) equate to the inverse of the modal mass of the fairing, and have units of 1/kg. The integral terms account for the translational force and rotational moment loads on the fairing.

We shall assume that the in-plane displacement of the fairing is not significant and does not contribute to its overall vibration response (Howard, 1999, Howard et al 1997). Only the out-of-plane vibration shall be considered in this analysis. Theoretically, there is a small degree of coupling from the in-plane vibration to the out-of-plane vibration; however the magnitude is small and can be ignored (Howard, 1999). Hence the following relationships can be used to describe the displacement of the fairing

$$U_{sk} = 0 \quad U_{\theta k} = 0 \quad U_{wk} = [\psi] \mathbf{w}_p \quad (7)$$

The mode shapes $[\psi]$ of the structure are calculated using the ANSYS finite element software, and $\mathbf{w}_p$ is the vector of modal participation factors. The force and moment loads on the fairing are assumed to be point loads, which can be described with Dirac delta functions. Making use of the relationship

$$\int_\alpha F(\alpha)\frac{\partial}{\partial\alpha}\left[\delta\left(\alpha-\alpha^*\right)\right]d\alpha = -\frac{\partial F(\alpha^*)}{\partial\alpha} \tag{8}$$

the integral in Eq. (3) can be evaluated as

$$F_k = \frac{1}{\Lambda_k}\left[[\psi_J]^T F_J - \frac{\partial[\psi_J]^T}{\partial y}M_{Jx} + \frac{\partial[\psi_J]^T}{\partial x}M_{Jy}\right] \tag{9}$$

where the modal mass is defined as

$$\Lambda_k = \rho h N_k \tag{10}$$

The rotations of the fairing about σ_J are given by (Leissa, 1973, Soedel, 1993)

$$\theta_s = \frac{v}{R} - \frac{1}{R}\frac{\partial w}{\partial\theta} \tag{11}$$

$$\theta_\theta = -\frac{1}{R}\frac{\partial w}{\partial s} \tag{12}$$

$$\theta_w = \frac{1}{2R^2}\left(R\frac{\partial v}{\partial s} - R\frac{\partial u}{\partial\theta}\right) \tag{13}$$

The partial differentials of the mode shapes $[\psi]$ with respect to the spatial co-ordinates are the mode shapes in the rotational directions. The ANSYS software calculates these rotational mode shapes, which can be extracted for use with the modal coupling software implemented in Matlab. Eq. (9) can be written as

$$F_k = \frac{1}{\Lambda_p}\left[[\psi_J]^T F_J - [\psi_{J\theta x}]^T M_{Jx} + [\psi_{J\theta y}]^T M_{Jy}\right] \tag{14}$$

where $[\psi_{J\theta x}]$ and $[\psi_{J\theta y}]$ are the rotational mode shapes about the θ_x and θ_y axes, respectively. These rotational mode shapes are calculated in ANSYS and are extracted and converted into units that are consistent with the translational mode shapes.

The rotational mode shapes from ANSYS are described using the global Cartesian coordinate system. The theoretical development in this section assumes that the rotational mode shapes are in an orthogonal coordinate system that has an axis normal to the surface of the structure.

Equations of Motion for Cantilevered Tuned Vibration Damper

One concept for a tuned vibration damper, which can transmit both translational forces and rotational moments, is a device that consists of point masses which are cantilevered from a central shaft (Ting-Kong, 1999, Hill et al., 2002a, Hill et al., 2002b). The resonance frequencies of the damper are adjusted by changing the lengths of the cantilever arms. This section contains the equations of motion of a dual cantilever vibration damper and the integration of these equations into the equations of motion of the structure developed later in this paper.

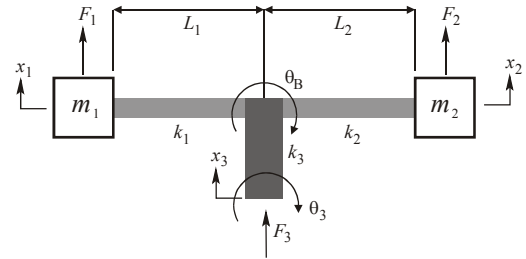Figure 2 shows a mathematical model of the two mass cantilevered tuned vibration damper.

Figure 2: Mathematical model of the two mass cantilevered tuned vibration dampers.

It is assumed that:

- Point masses are located on the ends of the cantilever arms.

- The rotation of the masses is negligible so the rotational inertia of the masses is ignored.

- The masses of the arms are negligible compared to the point masses and hence can be ignored from the point of view of the system dynamics.

- The central column has very high axial stiffness compared to the bending stiffness of the arms, so that the axial stiffness of the column can be assumed infinite.

- The central column has bending flexibility.

The tuned vibration damper has two masses m_1 and m_2 on the ends of cantilever arms that have lengths L_1 and L_2, respectively. The transverse stiffnesses of these arms, k_1 and k_2, are given by

$$k_1 = 3E_1I_1 / L_2^3 \tag{15}$$

$$k_2 = 3E_2I_2 / L_2^3 \tag{16}$$

where E and I are the Young's modulus and moment of inertia, respectively. The rotational stiffness of the upright central column is given by

$$k_3 = E_3I_3 / L_3 \tag{17}$$

Without going into the lengthy algebraic derivation of the equations of motion, it can be shown that the equations for the motion of the cantilever can be reduced into a matrix formulation as

$$\begin{bmatrix} A_{11} & A_{12} & A_{13} \\ A_{21} & A_{22} & A_{23} \\ A_{31} & A_{32} & A_{33} \end{bmatrix}\begin{bmatrix} x_1 \\ x_2 \\ x_3 \end{bmatrix} = \begin{bmatrix} F_1 \\ F_2 \\ (\sum_J [\psi_J]^T F_J \\ -[\psi_{J\theta x}]^T M_{Jx} \\ +[\psi_{J\theta y}]^T M_{Jy}) \end{bmatrix} \tag{18}$$

where the terms A_{11} to A_{33} are described in the Appendix.

Fully Coupled Vibro-Acoustic Model

This section describes the integration of the vibration response of the structure, which includes the effects of the cantilever vibration dampers, with the acoustic response of

the cavity, which includes the effects of the HRs, to result in equations that describe the coupled vibro-acoustic system.

The previous section described the equations of motion for the cantilevered vibration damper. The design proposed here involves using two of these devices orientated at 90 degrees to each other, as shown in Figure 3.
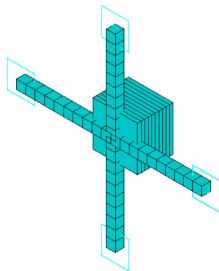

Figure 3: Picture of a four-armed cantilever TMD modelled in ANSYS. The masses on the end of the arms are indicated by the un-filled squares.

Hence the equations of motion for the structural system will contain two sets of the **A** matrices described in Eq. (18). The matrices for the structural equations will be

$$
\begin{bmatrix}
\begin{bmatrix} \mathbf{A}_{11}^{A} & \mathbf{A}_{12}^{A} \\ \mathbf{A}_{21}^{A} & \mathbf{A}_{22}^{A} \end{bmatrix} & \begin{bmatrix} \mathbf{0} & \mathbf{0} \\ \mathbf{0} & \mathbf{0} \end{bmatrix} & \begin{matrix} \mathbf{A}_{13}^{A} \\ \mathbf{A}_{23}^{A} \end{matrix} \\
\begin{bmatrix} \mathbf{0} & \mathbf{0} \\ \mathbf{0} & \mathbf{0} \end{bmatrix} & \begin{bmatrix} \mathbf{A}_{11}^{B} & \mathbf{A}_{12}^{B} \\ \mathbf{A}_{21}^{B} & \mathbf{A}_{22}^{B} \end{bmatrix} & \begin{matrix} \mathbf{A}_{13}^{B} \\ \mathbf{A}_{23}^{B} \end{matrix} \\
\begin{matrix} \mathbf{A}_{31}^{A} & \mathbf{A}_{32}^{A} \end{matrix} & \begin{matrix} \mathbf{A}_{31}^{B} & \mathbf{A}_{32}^{B} \end{matrix} & \mathbf{A}_{33}^{A} + \mathbf{A}_{33}^{B}
\end{bmatrix} \times
$$

$$
\begin{bmatrix} x_1^{A} \\ x_2^{A} \\ x_1^{B} \\ x_2^{B} \\ w_p \end{bmatrix} =
\begin{bmatrix}
F_1^{A} \\
F_2^{A} \\
F_1^{B} \\
F_2^{B} \\
\left(\sum_J [\psi_J]^{\mathrm{T}} F_J \right. \\
-[\psi_{J\theta x}]^{\mathrm{T}} M_{Jx} \\
\left. +[\psi_{J\theta y}]^{\mathrm{T}} M_{Jy} \right)
\end{bmatrix}
\tag{19}
$$

where w_p are the modal participation factors for the response of the structure, x_1 and x_2 are the displacements of the point masses attached to the ends of the cantilever arms and the superscript A and B refers to one pair of cantilevers as shown in Figure 2. The F_J term refers to the force applied to the structure, and the M_{Jx} and M_{Jy} terms refer to the moments applied to the structure.

It can be seen that the format of this matrix equation is similar to the **A** matrices in Howard et al. (2005). Hence it is possible to incorporate this matrix equation into the fully-coupled vibro-acoustic theory developed previously where the **A** sub-matrices can be replaced by

$$
\mathbf{A}_{11}' = \begin{bmatrix}
\begin{bmatrix} \mathbf{A}_{11}^{A} & \mathbf{A}_{12}^{A} \\ \mathbf{A}_{21}^{A} & \mathbf{A}_{22}^{A} \end{bmatrix} & \begin{bmatrix} \mathbf{0} & \mathbf{0} \\ \mathbf{0} & \mathbf{0} \end{bmatrix} \\
\begin{bmatrix} \mathbf{0} & \mathbf{0} \\ \mathbf{0} & \mathbf{0} \end{bmatrix} & \begin{bmatrix} \mathbf{A}_{11}^{B} & \mathbf{A}_{12}^{B} \\ \mathbf{A}_{21}^{B} & \mathbf{A}_{22}^{B} \end{bmatrix}
\end{bmatrix}
\tag{20}
$$

$$
\mathbf{A}_{12}' = \begin{bmatrix} \mathbf{A}_{13}^{A} \\ \mathbf{A}_{23}^{A} \\ \mathbf{A}_{13}^{B} \\ \mathbf{A}_{23}^{B} \end{bmatrix}
\tag{21}
$$

$$
\mathbf{A}_{21}' = \begin{bmatrix} \mathbf{A}_{31}^{A} & \mathbf{A}_{32}^{A} & \mathbf{A}_{31}^{B} & \mathbf{A}_{32}^{B} \end{bmatrix}
\tag{22}
$$

$$
\mathbf{A}_{22}' = \begin{bmatrix} \mathbf{A}_{33}^{A} + \mathbf{A}_{33}^{B} \end{bmatrix}
\tag{23}
$$

METHOD OF OPTIMISATION

As described in Howard et al. (2005), a semi-synchronous parallel genetic algorithm and a distributed computing network were used to optimise the locations and the parameters of the PVADs attached to the fairing. The distributed computing network is formed by the networking of about 280 desktop computers using the free software called Condor. The Condor software makes the resources of unused computers available to a pool. An attractive feature of this software is that if a person uses the computers in the pool, the Condor software immediately removes the job from the computer and re-starts the job on an unused computer.

The optimisations were conducted for 10 and 20 PVADs attached to the fairing. It was assumed that there was an identical mass on the end of each of the four arms on each PVAD, which together make up the total mass of the PVAD. The added mass to the fairing was set at 10% of the total mass of the fairing. The mass of the fairing is about 67kg. Hence the allowable added mass is about 6.7kg. If this is evenly divided into 20 PVADs, then each PVAD will weigh 335 grams, and the mass on the end of each of the four cantilever arms will be 84 grams. This is probably near the practical limits of a real cantilevered vibration damper. Hence the optimisation of 20 PVADs is the maximum number of dampers that was investigated.

The parameters were allowed to vary as listed in Table 1. In order to reduce the number of parameters to be optimised, the geometry of some of the components of the TMDs were fixed, as listed in Table 2.

Table 1: Parameter ranges for the PVADs used during the optimisation of the composite cylinder.

PVAD parameter	Min	Max	No. Values
PVAD position	1	5184	5184
Cantilever arm lengths (m)	0.01	0.1	500
Mass-spring damping (η)	0.01	0.25	10
Acoustic resonator frequency (Hz)	11	510	500
Acoustic resonator damping (η)	0.01	0.25	10

Table 2: Values for the cantilever vibration dampers.

Parameter	Value	Units	Comment
Young's modulus of arm	70.9	GPa	Aluminium
Moment of inertia of arm	52.08e-12	m^4	5mm diameter rod
Young's modulus of upright column	130	GPa	Stiff light-weight material
Moment of iertia of upright column	32.55e-9	m^4	25mm diameter rod

The acoustic loading on the fairing was assumed to be a plane harmonic wave incident at 90 degrees to the axis of the fairing as shown in Figure 4. The acoustic load has a cosine distribution around the circumference of the fairing (Potter, 1966).
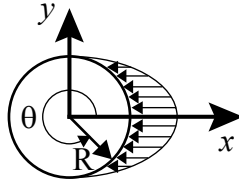
Figure 4: Mathematical model of the acoustic loads on the fairing.

The optimisations were conducted over 40,000 cost function evaluations of the acoustic potential energy inside the fairing. Each evaluation takes approximately 3 minutes on a single 3.0GHz desktop computer, which would total 83 days of computation time. By using the distributed computing network, the optimisations were completed in less than 4 days, with constant interruptions by people using computers in the Condor pool.

Figure 5 shows the gradual reduction in the total acoustic potential energy as the genetic algorithm determines the optimum parameters for the PVADs. The value of the total acoustic potential energy at the end of the optimisation process is approximately -23dB.
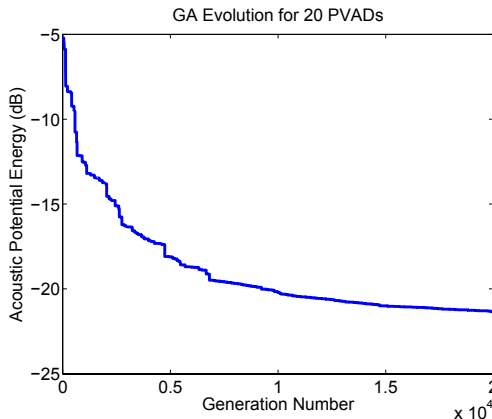
Figure 5: Evolution of the cost function during the optimisation using the genetic algorithm. Note that the number of cost functions evaluated is twice the generation number.

Figure 6 shows the corresponding acoustic potential energy versus frequency for the optimal configuration of the PVADs. Superimposed on these results is the acoustic potential energy inside the fairing when no PVADs were attached to the structure. Also shown on the graph are the equivalent resonance frequencies of the HRs and the TMDs. Note that as the TMDs have four resonance frequencies per PVAD, there are four times as many markers for the TMDs as the HRs. The results show that the use of the TMDs that has both

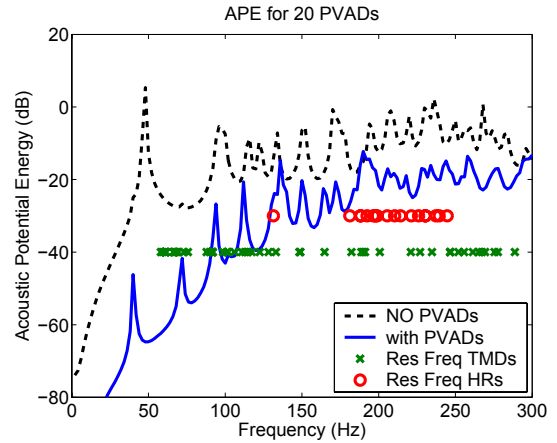translational and rotational degrees of freedom has improved the transmission loss of the fairing.

Figure 6: Acoustic potential energy versus frequency for the case of no PVADs; 20 PVADs comprising 20 four-armed cantilever TMDs and 20 HRs.

Figure 7 shows the distribution of the equivalent resonance frequencies of the TMDs and the HRs. These results show that even though the frequency range of interest was between 0 to 300 Hz, numerous resonance frequencies of the cantilevered TMDs which were outside the analysis range, still had an effect within the analysis range.
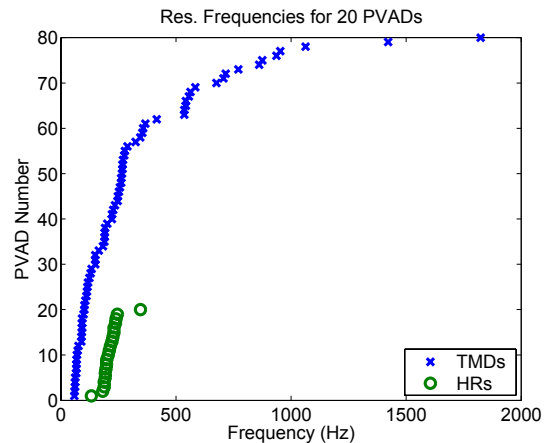
Figure 7: The equivalent resonance frequencies for the TMDs and the HRs.

Figure 8 shows the location of the PVADs on the fairing, displayed as if the fairing had been unwrapped. The 0 degrees marker is aligned with the incident sound wave.
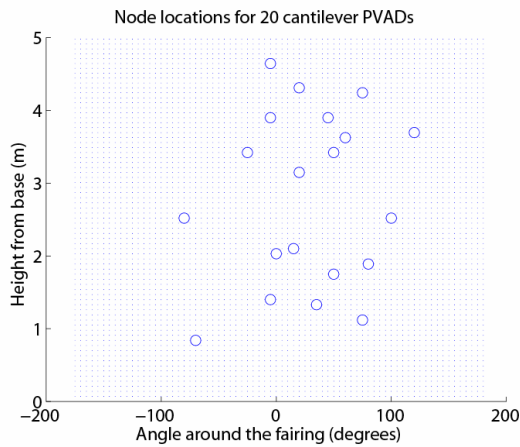
Figure 8: Locations of the 20 PVADs on the fairing shown by the circles. The dots indicate the potential location of the PVADs.

Figure 9 shows a comparison of the acoustic potential energies inside the fairing for the optimisation of the 20 PVADs comprising 20 four-armed cantilever TMDs and 20 HRs, and for 500 PVADs comprising 500 single-degree-of-freedom TMDs and 500 HRs. The 500 PVADs have the same total added mass budget as was used here for the analysis of the 20 PVADs with cantilever TMDs. The results show that the use of the 500 PVADs had the effect of 'smearing' the acoustic energy across the frequency range. The figure shows a reduction of energy at all frequencies and also shows that the 20 PVADs with the cantilever arms perform much better than 500 single-degree of freedom PVADs at low frequencies and equally or almost as well at high frequencies.
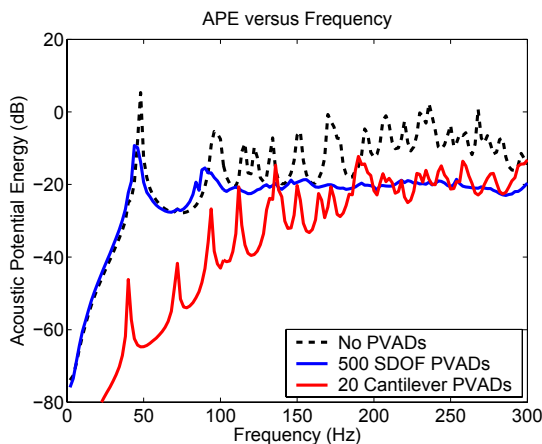

Figure 9: Acoustic potential energy versus frequency for the case where 500 PVADs comprising 500 single-degree-of-freedom TMDs, and 20 PVADs with four armed cantilever TMDs and 20 HRs.

Figure 10 shows the comparison of the total acoustic potential energy for 10, 100, and 500 PVADs with single degree of freedom TMDs, and 10 and 20 PVADs with four-armed cantilever TMDs. The results show that the 20 PVADs with cantilever TMDs provided the greatest noise control treatment for all the analyses considered, and resulted in the total acoustic potential energy inside the fairing of approximately -23dB.
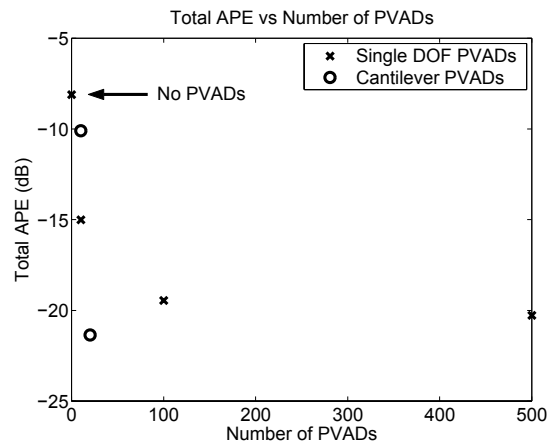

Figure 10: Comparison of the total acoustic potential energy for 10, 100, and 500 PVADs with single degree of freedom TMDs, and 10 and 20 PVADs with four-armed cantilever TMDs.

CONCLUSIONS

A mathematical model has been described for the coupling of a vibro-acoustic system to passive vibration absorbers, each comprising a passive acoustic absorbers and a four-armed cantilevered tuned-mass-damper that has both translational and rotational degrees of freedom. Analyses were conducted to determine the effectiveness of these passive vibration and acoustic absorbers as a noise control treatment for improving the transmission loss of a light-weight composite rocket payload fairing. The parameters for the PVADs were optimised by using a genetic algorithm and a distributed computing network. The results indicate that the use of the small number of multiple degree of freedom PVADs provided the greater noise reduction than many single degree of freedom PVADs. However, additional analyses are required to ensure that re-distribution of the acoustic energy does not create problems in other frequency bands, and that the noise control treatment is insensitive to variations in the acoustic loading of the fairing.

ACKNOWLEDGEMENTS

REFERENCES

Condor (2005), *The Condor Project Homepage*, University of Wisconson – Madison, USA, http://www.cs.wisc.edu/condor/.

Fahy, F. (1994), *Sound and Structural Vibration: Radiation, Transmission and Response*, Academic Press.

Futron Corporation (2002), *Space Transportation Costs: Trends in Price Per Pound to Orbit 1990--2000*, Futron Corporation, 7315 Wisconsin Avenue, Suite 900W, Bethesda, Maryland 20814, 301-913-9372, http://www.futron.com, 6 September.

Goldberg, D. (1989), *Genetic algorithms in search, optimization, and machine learning*, Addison-Wesley.

Griffin, S., Lane, S., & Leo., D. (2000), *Innovative vibroacoustic control approaches in space launch vehicles*. In Proceedings of Inter-noise 2000, 29th International Congress and Exhibition on Noise Control

Engineering, number paper no. 737, Nice, France, 27-30 August 2000. International Noise Control Engineering.

Henderson, B., Gerhart, C., Lane, S. & Jensen, E. (2003), *Vibro-acoustic launch protection experiment (VALPE)*. Journal of the Acoustical Society of America, 114(4):2384.

Hill, S., Snyder, S. & Cazzolato, B. (2002a), *An adaptive vibration absorber*. In Proceedings of the Annual Australian Acoustical Society Conference, Adelaide, Australia, Nov 13-15, pages 34-41.

Hill, S. & Snyder, S. (2002b), *Design of an adaptive vibration absorber to reduce electrical transformer structural vibration*. Transactions of the ASME, Journal of Vibration and Acoustics, 124(4):606-611.

Howard, C., Hansen, C. & Pan, J. (1997), *Power transmission from a vibrating body to a circular cylindrical shell through active elastic isolators*, Journal of the Acoustical Society of America 101(3), 1479–1491.

Howard, C. (1999), *Active vibration isolation of machinery vibration from flexible structures*, PhD thesis,

Department of Mechanical Engineering, University of Adelaide, Adelaide, South Australia, Australia.

Howard, C.Q., Hansen, C.H. & Zander, A.C. (2005), *Multi-Variable Optimisation of a Vibro-Acoustic System Using a Distributed Computing Network*, In: Proceedings of Acoustics 2005, 9-11 November 2005, Busselton, Western Australia

Leissa, A. W. (1973), *Vibration of shells*. SP-288. NASA.

Mathworks (2004), *Matlab compiler*, Mathworks, Natick, Massachusetts, USA http://www.mathworks.com/products/compiler/.

Potter, R. (1966), *Correlation patterns of the acoustic pressure fluctuations on the S-IC vehicle due to the exhaust noise of the test and launch stand*. Technical Report Wyle Labs Report WR 66-15, Contract NAS8-20073-1.

Soedel, W. (1993), *Vibration of Shells and Plates*. Marcel Dekker Inc, New York.

Ting-Kong, C. (1999), *Design of an adaptive dynamic vibration absorber*, Master's thesis, The University of Adelaide.

APPENDIX

$$A_{11} = \left[k_1 - \omega^2 m_1 - L_1^2 \frac{k_1^2}{\left(L_1^2 k_1 + L_2^2 k_2 - k_{3\theta} \right)} \right] \tag{24}$$

$$A_{12} = L_1 k_1 L_2 \frac{k_2}{\left(L_1^2 k_1 + L_2^2 k_2 - k_{3\theta} \right)} \tag{25}$$

$$A_{13} = -k_1 \frac{\left(\psi_J L_2^2 k_2 - k_{3\theta} \psi_J + L_1 \psi_J L_2 k_2 - k_{3\theta} L_1 \psi_{J\theta} \right)}{\left(L_2^2 k_2 + L_1^2 k_1 - k_{3\theta} \right)} \tag{26}$$

$$A_{21} = L_1 k_1 L_2 \frac{k_2}{\left(L_2^2 k_2 + L_1^2 k_1 - k_{3\theta} \right)} \tag{27}$$

$$A_{22} = \left[k_2 - \omega^2 m_2 - L_2^2 \frac{k_2^2}{\left(L_1^2 k_1 + L_2^2 k_2 - k_{3\theta} \right)} \right] \tag{28}$$

$$A_{23} = -k_2 \frac{\left(\psi_J L_1^2 k_1 - k_{3\theta} \psi_J + L_1 \psi_J L_2 k_1 + L_2 k_{3\theta} \psi_{J\theta} \right)}{\left(L_2^2 k_2 + L_1^2 k_1 - k_{3\theta} \right)} \tag{29}$$

$$A_{31} = k_1 \frac{\left(-\psi_{JT} L_2^2 k_2 + \psi_{JT} k_{3\theta} - \psi_{JT} L_2 k_2 L_1 + \psi_{J\theta T} L_1 k_{3\theta} \right)}{\left(k_1 L_1^2 - k_{3\theta} + L_2^2 k_2 \right)} \tag{30}$$

$$A_{32} = -k_2 \frac{\left(\psi_{JT} k_1 L_1^2 - \psi_{JT} k_{3\theta} + \psi_{JT} L_1 k_1 L_2 + \psi_{J\theta T} L_2 k_{3\theta} \right)}{\left(k_1 L_1^2 - k_{3\theta} + L_2^2 k_2 \right)} \tag{31}$$

$$A_{33} = \left[\left[\begin{array}{c} \psi_{JT} \left(L_2 k_2 k_{3\theta} - L_1 k_1 k_{3\theta} \right) \psi_{J\theta} \cdots \\ + \psi_{JT} \left[\begin{array}{c} k_2 L_1^2 k_1 - k_2 k_{3\theta} \\ + k_1 L_2^2 k_2 - k_1 k_{3\theta} \cdots \\ + 2 L_1 k_1 L_2 k_2 \cdots \end{array} \right] \psi_J \end{array} \right] + \left[\left[\left[\begin{array}{c} -k_{3\theta} k_1 L_1^2 - k_{3\theta} L_2^2 k_2 \cdots \\ -\omega^2 L_3^2 (m_2 + m_1) \left[\begin{array}{c} L_2^2 k_2 \cdots \\ + L_1^2 k_1 \cdots \\ -k_{3\theta} \end{array} \right] \psi_{J\theta} \cdots \\ + k_{3\theta} \psi_J L_2 k_2 - k_{3\theta} L_1 k_1 \psi_J \end{array} \right] \psi_{J\theta T} \cdots \right] \right] \right] \frac{1}{\left(k_1 L_1^2 - k_{3\theta} + L_2^2 k_2 \right)} \tag{32}$$